
Article:
Xu, J., Zhu, D., Ibrahim, A.D. et al. (5 more authors) (2017) Raman Deuterium Isotope Probing Reveals Microbial Metabolism at the Single-Cell Level. Analytical Chemistry, 89 (24). pp. 13305-13312. ISSN 0003-2700

https://doi.org/10.1021/acs.analchem.7b03461

Raman-DIP (Deuterium Isotope Probing) Reveals Microbial Metabolism at the Single-Cell Level

Journal:	*Analytical Chemistry*
Manuscript ID	ac-2017-034615.R1
Manuscript Type:	Article
Date Submitted by the Author:	n/a

Complete List of Authors:	Xu, Jiabao ; University of Oxford Zhu, Di; University of Sheffield Ibrahim, Aliyu; Queen's University Belfast Allen, Christopher; Queen's University Belfast Gibson, Christopher; University of Sheffield, Department of Chemistry Fowler, Patrick; University of Sheffield, Chemistry Song, Yizhi; University of Oxford, Department of Engineering Science Huang, Wei; University of Oxford, Department of Engineering Science

Raman-DIP (Deuterium Isotope Probing) Reveals Microbial Metabolism at the Single-Cell Level

Jiabao Xu[1 Ψ], Di Zhu[2 Ψ], Aliyu D. Ibrahim[3], Christopher C. R. Allen[3], Christopher M. Gibson[4], Patrick W. Fowler[4], Yizhi Song[1] and Wei E. Huang[1, 2]*

1. Department of Engineering Science, University of Oxford, Parks Road, Oxford, OX1 3PJ, United Kingdom.

2. Kroto Research Institute, University of Sheffield, S3 7HQ, United Kingdom

3. School of Biological Sciences & Institute for Global Food Security, Queen's University Belfast, Belfast BT9 7BL, United Kingdom

4. Department of Chemistry, University of Sheffield, Sheffield S3 7HF, United Kingdom

[Ψ]Authors contribute equally to this study.

*Corresponding author: Wei E. Huang

wei.huang@eng.ox.ac.uk

Telephone: +44 (0)1865 283786, Fax: +44 (0)1865 3749

ABSTRACT

We illustrate that single-cell Raman microspectroscopy, coupled with deuterium isotope probing (Raman-DIP), provides a culture-independent and non-destructive approach to probe metabolic pathways of carbon substrates at the single-cell level. We find a distinguishable C-D vibration band at 2070 - 2300 cm^{-1} in single-cell Raman spectra (SCRS) when *Escherichia coli* used deuterated glucose and *Pseudomonas sp.* used deuterated naphthalene as sole carbon sources. The intensity of the C-D band is proportional to the extent of deuteration in carbon source, and as low as 5% deuteration can be distinguished by analysis of SCRS. It suggests that Raman-DIP could be used to semi-quantitatively and sensitively indicate metabolisms of deuterated carbon source in microbes. A lower lipid conversion rate of deuterated naphthalene compared to that of deuterated glucose was observed, presumably owing to different anabolic pathways and membrane alteration. Apart from C-D band shift from C-H, SCRS also reveal several isotopic shifts of phenylalanine band of which the positions correlate well with a computational model. A reduction in phenylalanine deuteration in *Pseudomonas sp.* compared to that in *E. coli* is due to dilution effect of deuterated carbon source via different phenylalanine pathways in *Pseudomonas sp.*. Collectively, we demonstrate that Raman-DIP can not only indicate metabolic activity using deuterated carbon sources, but also reveal different metabolic pathways by analysing SCRS. Harnessing such low-cost and versatile deuterated substrates, Raman-DIP has the potential to probe a wide range of metabolic pathways and functions at the single cell level.

Keywords: Raman microspectroscopy, single cell, pathway, stable isotope, carbon source, deuterium, metabolism

INTRODUCTION

Microorganisms play important roles in almost all ecosystems including natural environment and human body; and are extremely abundant and versatile on earth. New generations of sequencing technologies usually provide phylogenetical diversity and metagenomic profiling of microbial communities, but metabolic functions of individual microbes and their molecular mechanism are often elusive owing to the limited culturability and complexity of microbial communities[1,2]. Complementary to genomic approaches, stable isotope probing (SIP) and molecular biological methods enables functional and metabolic studies of microbes by a cultivation–independent way[3]. By exposing microbes to isotopically labelled substrates designed to mimic as closely as their naturally more abundant counterpart, it provides a direct link between microbial identities and their functions without altering the natural substrate pool. SIP has been extensively used in combination with mass spectrometry (MS) and nuclear magnetic resonance (NMR) spectroscopy to identify and quantify metabolites with high sensitivity[4]. However, these bulk analyses of cell populations obscure at times the high heterogeneity within microbial communities. Secondary ion mass spectrometry (SIMS), although known to provide high sensitivity and single-cell resolution, is limited in application by its destructive and expensive nature.

Among SIP-related techniques, the combination of single-cell Raman micro-spectroscopy and SIP enables non-destructive functional studies of microorganisms labelled with stable isotopes at a single-cell level[2]. Single-cell Raman spectra (SCRS) are regarded as biochemical fingerprints of single cells, which provide a snapshot of the intrinsic complex phenotypes[5]. Following the first observation of phenylalanine Raman band shifts in ^{13}C-glucose labelled bacterial cells[5], various isotope-labelled substrates have been used to exploit the potential of single-cell functions[2,6-10]. Manen et al. reported Raman-SIP detection of isotope-labelled protein using D-labelled phenylalanine, tyrosine and methionine in single HeLa cells[11]. By using a mixture of ^{12}C- and ^{13}C- glucose, Li et al. observed the Raman shifts of phenylalanine and thymine in the carbon flow from bacterial prey to its predators[12]. Berry et al. developed a universal Raman-SIP method using D_2O to measure general metabolic activities of single microbial cells[13]. Stiebing et al. visualised lipid uptake and storage within single macrophages using deuterated fatty acids[14]. Providing a high variety of possible isotopic substrates, Raman-SIP has the potential to probe cell activity and cellular metabolism of a broad range of important biomolecules including proteins, lipids, carbohydrates and nucleic acids.

It has been found that Raman microspectroscopy gives sensitive detection of the incorporation of deuterium in single cells[8,13], as a significant Raman shift in carbon-deuterium (C-D) vibration from C-H exhibits a clear and strong band at the 'silent zone' in SCRS which has no detectable Raman bands in most, if not all, cells growing with naturally abundant elements (e,g, ^{1}H, ^{14}N, ^{16}O and ^{12}C)[2]. Deuterated carbon sources can be synthesised by hydrogen-deuterium exchange reactions in the presence of D_2O, which is not only much more cost-effective than ^{13}C-substrates, but also able to make complex substrate or mixed compounds[15-17]. Hence, Raman-SIP with deuterated carbon source might be a cost-effective and sensitive approach to link cell to their carbon metabolism.

In this study, we applied Raman-DIP (deuterium isotope probing) to study the assimilation of specific deuterated carbon substrates such as glucose and naphthalene into lipid and protein compounds in single microbial cells. We used a mixture of glucose/glucose-d_{12} or naphthalene/naphthalene-d_8 to probe various anabolic pathways of carbon sources and semi-quantify the biosynthesis of fatty acids and phenylalanine in single cells of *E. coli* and *P. putida*. Given its ability to probe metabolic metabolism, we believe Raman-SIP can provide culture-independent insights in understanding the complex physiological systems of microbial communities.

EXPERIMENTAL SECTION

Bacterial strains, culture conditions, and plasmid transfer. For all strains tested, media were supplemented with carbon sources containing different ratios of D-glucose (Sigma Co, UK, D9434) to D-glucose-d_{12} (Sigma Co, UK, 616338) in water, or naphthalene (Sigma Co, UK, 84679) to naphthalene-d_8 (Sigma Co, UK, 176044) dissolved in dimethyl sulfoxide (DMSO). Pure cultures of *Escherichia coli* DH5α were grown aerobically overnight with 150 rpm shaking at 37 °C in M9 minimal medium with 10 mM glucose as the sole carbon source. Cultures of *Pseudomonas putida* strains UWC1 and G7 were grown aerobically for 72 hours with 150 rpm shaking at 30 °C in M9 medium with 10 mM naphthalene or glucose as the sole carbon source. OD_{600} were measured during cultivation with deuterated carbon sources.

Pseudomonas fluorescens WH2 contains pWH2-Nah plasmid carrying the naphthalene-degradation operon and the plasmid was transferred via conjugation from *P. fluorescens* WH2 to *P. putida* UWC1 (Table 1). Briefly, *P. fluorescens* WH2 and *P. putida* UWC1 were grown in LB medium overnight at 30 °C. One hundred μL of each were mixed and added on a 0.22 μm membrane filter (47 mm diameter, Millipore UK) placing on a LB agar plate,

followed by incubation at 30 °C for 16 hours. The bacterial biofilm grown on the filter was taken out and resuspended in 5 mL of PBS by vortex. Transconjugants bearing the naphthalene-degradation plasmid pWH2-Nah were selected in M9 minimal medium with 100 μg/mL rifampicin and naphthalene as the sole carbon source. As *P. putida* UWC1 cannot assimilate naphthalene but is rifampicin resistant (Table 1); and *P. fluorescens* WH2 doesn't resist rifampicin, only the transconjugants can grow on the selective plates. Colony PCR was performed to amply 16S-rRNA of the transconjugants using primers 63f and 1387r[18]. The transconjugants *Pseudomonas putida* UWC1 (pWH2-Nah$^+$) were confirmed by DNA sequencing of the PCR product.

Single-cell Raman spectra (SCRS) measurements and analysis. Samples were diluted to a concentration of ~ 1000 cells mL^{-1} and spotted onto an aluminium-coated slide. Individual cells were observed under a 100×/0.9 microscope objective. Individual single-cell spectra were acquired using an HR Evolution confocal Raman microscope (Horiba Jobin-Yvon) equipped with a 532 nm neodymium-yttrium aluminium garnet laser and 300 grooves/mm diffraction grating. The 1 μm^2 laser spot was used on single cells with a 4.7 mW laser power. The spectra were acquired in the range of 500 to 3500 cm^{-1} and the acquisition time was 10 s per spectrum. 30 single cells were analysed in each sample. All spectra were processed using LabSpec 5 (Horiba) with baseline correction and normalisation. Intensity of each band was quantified by calculating area under curve with baseline subtraction.

SCRS were used to quantify intracellular deuterium content originating from deuterated carbon sources. The C-D (2070 - 2300 cm^{-1}) and C-H (2800-3030 cm^{-1}) band areas were calculated by integrating single-cell spectra. The ratio of C-D / (C-D + C-H) was used to indicate the extent of deuterium incorporation from deuterated carbon source [8,13].

Calculation of Raman frequencies of phenylalanine. The equilibrium geometry of the palmitic acid molecule was calculated at the B3LYP/6 31G** level of theory using GAUSSIAN09. The conformer obtained had C_s point group symmetry, with the aliphatic backbone lying in the single mirror plane. Wavenumbers of Raman-active vibrations were then calculated for various substitution patterns on the molecular backbone, including all-H and all-D forms, the distinct single-D substitutions in the all-H form, the distinct single-H substitutions in the all-D form, and full deuteration along half the length of the backbone, starting from either methyl or carboxylic termini. Examples of calculated Raman spectra are shown in Figure S3.

Raman wavenumbers of phenylalanine were then calculated at the same level for 32 possible isotopomers obtained by H/D substitution on the phenyl ring. The 'ring breathing' vibration at 1017 cm^{-1} in the 'all H' structure was identified as the match for the experimental peak at 1004 cm^{-1}, as it was the only intense peak in that region of the spectrum. The data from each of the 32 structures was then grouped by %D in the ring (i.e., 0, 20, 40, 60, 80 and 100%, depending on whether there were 0, 1, 2, 3, 4 or 5 D on the ring), and further grouped by mirror symmetry to account for the approximately free rotation about the ring-backbone bond.

RESULTS AND DISCUSSION

Raman-DIP sensitively detected carbon metabolism by using deuterated carbon sources.

Both *E. coli* DH5α and *P. putida* UWC1 are able to use glucose as the sole carbon source[19]. Figure 1a and 1b show SCRS of *E. coli* DH5α and *P. putida* UWC1 grown overnight in glucose as sole carbon source with different percentages of fully deuterated glucose-d_{12}. With the presence of deuterated glucose, a distinguishable Raman band appeared in the region between 2070 and 2300 cm^{-1} in SCRS, and this broad band was attributed to C-D stretching vibrations[2,13]. The intensity of this C-D band was enhanced while that of the C-H band at 2800 – 3100 cm^{-1} was reduced with increasing percentage of deuterated glucose-d_{12} in the growth media. This spectral pattern demonstrates exchanges of intracellular H by D due to metabolism of deuterated carbon sources (Fig. S2).

Pseudomonas fluorescens WH2 and *P. putida* G7 are two bacteria capable of utilising naphthalene as sole carbon and energy source. The naphthalene-degradation trait is conferred by plasmid pWH2-Nah in *P. fluorescens* WH2[9] and NAH7 in *P. putida* G7[20]. *P. putida* UWC1 received pWH2-Nah plasmid by conjugation with *P. fluorescens* WH2, obtaining the ability to metabolise naphthalene. Figure 1c and 1d show SCRS of *P. putida* UWC1 (pWH2-Nah^{+}) and *P. putida* G7 (NAH7) grown in naphthalene as the sole carbon source with different percentages of fully deuterated naphthalene-d_8. Similar to deuterated glucose-d_{12} metabolism shown above, the intensity of the C-D band proportionally increased with increasing percentage of deuterated naphthalene-d_8 in the growth medium. Controls of *P. putida* UWC1 (pWH2-Nah^{+}) without naphthalene and *P. putida* UWC1 with 100% naphthalene-d_8 displayed a flat and 'silent' C-D region between 2070 and 2300 cm^{-1} in SCRS and no increase in OD_{600} after incubating for 72 hours (Fig. S1), ruling out any solvent effect or abiotic H-D exchanges in the cells.

Deuterium and hydrogen are chemically identical as deuteration has negligible effect on atom size, molecular shape, equilibrium bond length or stiffness[21], apart from small vibrational effects. Deuteration does however influence Raman positions for spectral modes in which the H/D atom is moving, and kinetics of reactions in which the H/D atom is involved. Therefore, we assume that, to some extent, cells are unable to distinguish between undeuterated carbon sources (glucose and naphthalene) and fully deuterated carbon sources (glucose-d_{12} and naphthalene-d_8) in carbon metabolism. Figure 2 shows the growth curves of microbes in the presence of different percentages of deuterated carbon sources. The three *P. putida* strains UWC1, UWC1 (pWH2-Nah$^+$) and G7 were unable to distinguish deuterated and undeuterated glucose/naphthalene and exhibited no growth differences among conditions from 0 - 100% deuterated glucose and naphthalene ($p > 0.01$). There was no significant observable effect on the growth kinetics of *E. coli* grown in 0 - 100% deuterated glucose in the initial 6 hours ($p = 0.058$). Although 0 - 75% deuterated glucose conditions featured indistinguishable growth curves, 100% deuterated glucose exhibited a repressed stationary phase compared to other less deuterated glucose. It is unclear why it happened.

Formation of a C-D bond in a deuterated carbon source is passed to $NADP^+$ to form NADPD, which is then used to form a new C-D bond during reduction reactions to synthesise cellular building blocks (e.g. lipids) (Fig. S2). This C-D bond leads to a clearly distinguishable broad band at 2070 - 2300 cm^{-1} in SCRS. Figure 3 shows that the intensity ratio of C-D / (C-D + C-H) in SCRS and the percentage of deuterated carbon source followed a linear relationship in all four cases, regardless of carbon source and bacterial species. It suggests that cells should statistically incorporate D from deuterated carbon source into cells, proportional to the percentage of deuterated carbon source in the medium. This result is in good agreement with our hypothesis that cells cannot distinguish deuterated carbon sources from their unlabelled counterparts. The SCRS demonstrate a sensitive D detection limit at as low as 5% deuterated glucose ($p < 0.001$) and 5% deuterated naphthalene ($p < 0.01$) (Fig. 3).

Calculations on the palmitic acid molecule as a typical fatty acid (Fig. S3) were used to shed further light on the above spectral observations. In summary: the stretches of C-H / C-D bonds on the aliphatic backbone are found to be effectively decoupled from other molecular vibrations. Each D substitution in a CH_2 or CH_3 group of the backbone produces an extra contribution to the band in the C-D stretch region (~2150 – 2350 cm^{-1} in the calculated spectrum, corresponding to an overestimation by a few percent of the vibrational force constant) and removes intensity from the C-H stretch region (~2950 – 3150 cm^{-1} in the

calculated spectrum), as predicted by the $\sqrt{2}$ rule arising from reduced mass effects, and with the contribution of each C-H and C-D to band area being in approximately 2:1 ratio. The effects of D substitution are more or less independent of the number and position of substitutions on carbon atoms of the backbone. Thus, the spectral intensities could be used to estimate C-D/C-H ratios here and in similar aliphatic environments.

Although lipids synthesis plays the most important part in the D incorporation at 2070 - 2300 cm^{-1} as it contributes roughly 20-35% to the total cellular C-H content[13], theoretically, C-D Raman band can include any possible C-D vibrations in lipids, proteins, nucleic acids and carbohydrates. Our results suggest that this process is a ubiquitous metabolic process which can be sensitively detected by SCRS. Taken together, a deuterated carbon source can be used as a universal indicator to probe carbon utilisation.

Raman-DIP revealed distinct biosynthesis pathways of fatty acids starting from different deuterated carbon sources.

In Figure 3, despite showing a linear relationship under both glucose and naphthalene conditions, the slopes of the lines are significantly different ($p < 0.001$). When the cells were grown in 100% glucose-d_{12} as the sole carbon source, the ratio of C-D / (C-D + C-H) was 21.7% in *E. coli* and 29.0% in *P. putida* UWC1. However, when 100% naphthalene-d_8 was used as the sole carbon source, the ratio decreased greatly, to 5.7% in *P. putida* UWC1 (pWH2-Nah^+) and 3.5% in *P. putida* G7. As lipid biosynthesis contributes roughly 20-35% to the total cellular C-H content[13], it plays a crucial part in the appearance of the broad C-D band through different lipid catabolic pathways degrading glucose or naphthalene (Fig. 4). The glycolytic conversion of fatty acids from carbohydrates generates a common intermediate phosphoenolpyruvate (PEP) through both Embden-Meyerhof-Parnas (EMP) and Entner-Doudoroff (ED) pathways in *E. coli*[22] and almost exclusively through the ED route in *P. putida*[23]. The aerobic degradation of naphthalene, however, proceeds in more steps involving two-stage cleavages of aromatic rings in naphthalene[24]. The first cleavage stage produces a central intermediate – salicylate, which is further converted to catechol[25]. This is followed by the second stage which includes ring fission by either ortho-cleavage between the hydroxyl groups or meta-cleavage adjacent to one of the hydroxyls[25]. The resulting intermediates then get into central metabolism to produce TCA cycle intermediates such as acetyl-CoA, succinyl-CoA, oxaloacetate and pyruvate. Hence, the pathway to make key metabolites for fatty acids synthesis via naphthalene metabolism in microbes is involved in more anabolic steps than that via glucose metabolism (Fig. 4). A significant amount of D in

original naphthalene-d_8 substrate was gradually lost during the ring-cleavage reactions, which contributed to the lower intensity ratio of C-D / (C-D + C-H) observed in the cells grown with deuterated naphthalene than those grown with deuterated glucose in *P. putida* UWC1 (Fig. 3). This pattern was not limited to *P. putida* UWC1 grown in deuterated glucose and naphthalene. It was also true in other strains such as *E. coli* DH5a grown in deuterated glucose and *P. putida* G7 grown in deuterated naphthalene (Fig. 3), which collectively validates the mechanistic explanation in Figure 4. Furthermore, it has been previously reported that the structure and composition of fatty acids changed in microorganisms grown with aromatic compounds as a sole carbon source[26]. An increase in the saturation/unsaturation ratio in naphthalene-grown cells compared to glucose-grown cells was found in *P. putida*, *P. stutzeri*, *P. vesicularis* and *Pseudomonas* sp. JS150[27,28]. This increase in membrane lipid saturation is consistent with the application of a previously postulated adaptive mechanism to compensate the fluidising toxicity on bacterial membranes caused by many aromatic compounds such as naphthalene, benzene, phenol and catechol[29,30]. It leads to less C-H bonds in lipids when cells were grown in naphthalene, further reducing C-D bonds observed in SCRS. In summary, the intensity ratio of C-D / (C-D + C-H) is dependent on the degree of cellular H/D exchanges which stems from different deuterated carbon sources, proceeds through various numbers of metabolic steps, and finally yields essential metabolites for lipid biosynthesis.

Raman-DIP revealed distinct biosynthesis pathways of phenylalanine starting from different deuterated carbon sources.

In addition to the C-D spectral feature observed in SCRS at 2070 - 2300 cm^{-1}, isotopic shifts were also observed at 1004 cm^{-1} which can be assigned to the aromatic amino acid phenylalanine (Fig. 1 and Fig. 5). Figure 5 highlights the Raman shift around 1004 cm^{-1} in a magnified view between 940 – 1020 cm^{-1} in Figure 1. Here we observe the shifts from 1004 cm^{-1} to 988, 976 and 962 cm^{-1} when cells were grown with deuterated glucose (Fig. 5). This is in a good agreement with a previous study of *Geobacter metallireducens* grown with deuterated acetate, observing a splitting pattern of phenylalanine Raman band[7]. However, the shifts were absent when cells were grown with deuterated naphthalene (Fig. 5). To understand the observed shifts of phenylalanine band, we calculated the equilibrium geometry and Raman frequencies for 32 possible isotopomers of phenylalanine depending on different D substitutions on the phenylalanine ring (Table S1). This results in a total of 4 possible Raman positions of the H/D mixture at 1004, 989-990, 976 and 962-963 cm^{-1} (Table

S1, Fig. S4, and Fig. S5), which correlate well with the experimental band positions (Table S2). The theoretical calculation also offers a good explanation for the differences in isotopic shifts with respect to different D percentages. Owing to the form of the vibrational mode, in which the motion is a three-fold asymmetrical breathing of three C-H (or C-D) units against the rest of the molecular framework, with little participation of the remaining ring C-H units. Substitutions at only three sites on the phenyl ring (sites 1, 3 and 5) are found to affect the position of the vibration (Fig. S4). The bands at 1004 cm^{-1} correspond to structures where sites 1, 3 and 5 are H, and so can occur when some D is present in the sample. The bands at 989-990 cm^{-1} occur when any of the sites 1, 3 and 5 are D. The bands at 976 cm^{-1} occur when any two of the sites 1, 3 and 5 are D, and therefore only present at higher D/H ratios. The bands at 962 correspond to structures where sites 1, 3 and 5 are D, and hence can only appear at D/H ratios above 60%, which correlates nicely with the observation that the bands at 962 cm^{-1} were only present under conditions with 75% and 100% deuterated glucose (Fig. 5a and 5b). The wavenumber shifts of 3%, 6% and 9% are consistent with the effect of changing the mass of the small units vibrating harmonically against a rigid framework, where each active D contributes additively to the higher effective mass for the vibration, and hence gives rise to a square root dependence in mode wavenumbers.

We then quantified the degree of D incorporation by calculating the ratio of total D to total H and D as following, in which *A* represents the area under the curve centred at a defined wavenumber:

$$\text{Total } \frac{D}{D+H} = \frac{A_{962\ cm^{-1}} + \frac{2}{3} \times A_{976\ cm^{-1}} + \frac{1}{3} \times A_{989\ cm^{-1}}}{A_{976\ cm^{-1}} + A_{989\ cm^{-1}} + A_{1004\ cm^{-1}}}$$

A high variability of the cellular D content at the same level of deuterated carbon source was observed between carbon sources and between species. In Figure 6, linearity is found between D percentage and cellular D uptake under the conditions with glucose. However, *E. coli* grown in 100% deuterated glucose-d_{12} displays a much higher D incorporation (58.1%) than *P. putida* UWC1 in the same carbon source (28.3%). This can be explained by the less efficient utilisation of glucose in *P. putida* compared to *E. coli* (Fig. 7a and 7b). The catabolism of glucose in *E. coli* DH5α has been proven mainly via the EMT pathway and the phosphotransferase (PTS) system, in which glucose is phosphorylated to glucose-6P and eventually converted to phosphoenolpyruvate (PEP) for the synthesis of aromatic amino acids via the shikimate pathway[31] (Fig. 7a). In contrast, it is reported that bacteria of *Pseudomonas*

spp. catabolise glucose almost exclusively through the ED pathway[32,33] (Fig. 7b). This pathway in *P. putida* involves three simultaneous sub-pathways starting with glucose, gluconate or 2-keto-gluconate that converge at the level of 6-phosphogluconate (6PG)[34]. 6PG is further converted to a key intermediate 2-keto-3-deoxy-6-phosphogluconate (KDPG) and continues to the production of PEP. The interconversion and cellular transportation of glucose, gluconate and 2-keto-gluconate in three convergent pathways might largely contribute to the D loss observed in SCRS of *Pseudomonas* bacteria grown with deuterated glucose. On the other hand, when deuterated naphthalene was used as the sole carbon source, no shifts of the phenylalanine band at 1004 cm^{-1}, presumably caused by D incorporation, was detected in *P. putida* UWC1 (pWH2-Nah^{+}) and *P. putida* G7 cells (Fig. 5c and 5d). These cells were unable to directly convert naphthalene into shikimate pathway intermediates before entering central metabolism cycle (Fig. 7c). D in naphthalene was largely lost during the two-phase ring cleavage processes and further diluted in the TCA cycle before D was used to form phenylalanine. Therefore, D in naphthalene-d_8 was largely lost due to many dilution steps in naphthalene pathway (Fig. 7c), whilst D is less diluted and remained in intermediate metabolites to make phenylalanine in glucose metabolic pathway (Fig. 7a and 7b). Our results suggest that Raman-DIP could indicate relative numbers of dilution steps in metabolic pathways by analysing isotopic shifts of the phenylalanine band in SCRS.

Advantages of Raman-DIP in metabolic studies by using deuterated carbon source

Raman-DIP has advantages over other analytical technologies of SIP in terms of its non-destructive nature, high isotopic sensitivity (detection limit at ~5% deuteration) and single-cell level detection. Its non-destructive nature offers possibilities for downstream single-cell sorting and omics (e.g. single cell genomics) analysis[2,35]. When combining with metabolic studies, it has the potential to provide a culture-independent approach to probe metabolic activity at the single-cell level in complex microbial communities. In SIP practice, ^{13}C-labelled or ^{15}N-labelled derivatives of substrates are generally expensive and a lot of them are not commercially available, which limits their use in Raman-SIP studies. This problem can be overcome by using much less expensive deuterated carbon substrates, as these deuterated compounds can be synthesised more efficiently and more cost effectively by H/D exchange reactions in D_2O environment[16]. The relatively low cost and high versatility of D-labelled substrates allows a wider applicability to make a broad range of complex deuterated substances including natural products, medicines, and deuterated mixtures containing

multiple chemicals. Raman-DIP using these D-labelled substrates is therefore invaluable in the functional studies of microbial cells in their natural habitats at the single-cell level.

CONCLUSIONS

We demonstrate that Raman-DIP is able to probe metabolic pathways at the single-cell level using deuterated carbon sources. By culturing microbes in deuterated glucose and naphthalene, we observed an isotopic Raman shift from C-H to C-D and the intensity of the C-D band can be used as an indicator of microbial carbon utilisation. The differences in cellular D uptake were due to different metabolic pathways of glucose and naphthalene. It is found that the isotopic Raman shifts at phenyl ring vibration are related to dilution steps of deuterated substrates in different metabolic pathways. A mathematical model was developed to calculate the D content in phenylalanine and its variation was dependent on different metabolic pathways. This study unveils the potential of Raman-DIP in the metabolic and functional study of microbial cells using low-cost and versatile D-labelled substrates.

ACKNOWLEDGEMENT

WEH acknowledges support from EPSRC (EP/M002403/1 and EP/M02833X/1) and NERC (NE/M002934/1) in the UK. CMG thanks EPSRC and the University of Sheffield for support under a GTA studentship.

SUPPORTING INFORMATION

Details on control Raman spectra, control growth kinetics, biological mechanism, phenylalanine structure and computational calculations included in supplementary figures (Figure S1-S5) and tables (Table S1-S2).

REFERENCE

(1) Robinson, C. J.; Bohannan, B. J. M.; Young, V. B. *Microbiol Mol. Biol. Rev.* **2010**, *74*, 453-76.
(2) Wang, Y.; Huang, W. E.; Cui, L.; Wagner, M. *Curr. Opin. Biotechnol.* **2016**, *41*, 34-42.
(3) Radajewski, S.; Ineson, P.; Parekh, N. R.; Murrell, J. C. *Nature* **2000**, *403*, 646-649.
(4) Tang, J. *Curr. Genomics* **2011**, *12*, 391-403.
(5) Huang, W. E.; Griffiths, R. I.; Thompson, I. P.; Bailey, M. J.; Whiteley, A. S. *Anal. Chem.* **2004**, *76*, 4452-4458.
(6) Huang, W. E.; Stoecker, K.; Griffiths, R.; Newbold, L.; Daims, H.; Whiteley, A. S.; Wagner, M. *Environ. Microbiol.* **2007**, *9*, 1878-1889.
(7) Kubryk, P.; Kolschbach, J. S.; Marozava, S.; Lueders, T.; Meckenstock, R. U.; Niessner, R.; Ivleva, N. P. *Anal. Chem.* **2015**, *87*, 6622-6630.

(8) Wang, Y.; Song, Y.; Tao, Y.; Muhamadali, H.; Goodacre, R.; Zhou, N. Y.; Preston, G. M.; Xu, J.; Huang, W. E. *Anal. Chem.* **2016**, *88*, 9443-9450.
(9) Huang, W. E.; Ferguson, A.; Singer, A. C.; Lawson, K.; Thompson, I. P.; Kalin, R. M.; Larkin, M. J.; Bailey, M. J.; Whiteley, A. S. *Appl. Environ. Microbiol.* **2009**, *75*, 234-241.
(10) Li, M.; Canniffe, D. P.; Jackson, P. J.; Davison, P. A.; FitzGerald, S.; Dickman, M. J.; Burgess, J. G.; Hunter, C. N.; Huang, W. E. *ISME J.* **2012**, *6*, 875-885.
(11) van Manen, H. J.; Lenferink, A.; Otto, C. *Anal. Chem.* **2008**, *80*, 9576-9582.
(12) Li, M.; Huang, W. E.; Gibson, C. M.; Fowler, P. W.; Jousset, A. *Anal. Chem.* **2013**, *85*, 1642-1649.
(13) Berry, D.; Mader, E.; Lee, T. K.; Woebken, D.; Wang, Y.; Zhu, D.; Palatinszky, M.; Schintlmeister, A.; Schmid, M. C.; Hanson, B. T.; Shterzer, N.; Mizrahi, I.; Rauch, I.; Decker, T.; Bocklitz, T.; Popp, J.; Gibson, C. M.; Fowler, P. W.; Huang, W. E.; Wagner, M. *Proc Natl. Acad. Sci. U. S. A.* **2015**, *112*, E194-203.
(14) Stiebing, C.; Matthaus, C.; Krafft, C.; Keller, A. A.; Weber, K.; Lorkowski, S.; Popp, J. *Anal. Bioanal. Chem.* **2014**, *406*, 7037-7046.
(15) Gant, T. G. *J. Med. Chem.* **2014**, *57*, 3595-3611.
(16) Atzrodt, J.; Derdau, V.; Fey, T.; Zimmermann, J. *Angew. Chem. Int. Ed. Engl.* **2007**, *46*, 7744-7765.
(17) Junk, T.; Catallo, W. J. *Chem. Soc. Rev.* **1997**, *26*, 401-406.
(18) Marchesi, J. R.; Sato, T.; Weightman, A. J.; Martin, T. A.; Fry, J. C.; Hiom, S. J.; Wade, W. G. *Appl. Environ. Microbiol.* **1998**, *64*, 795-799.
(19) Nikel, P. I.; Chavarria, M.; Fuhrer, T.; Sauer, U.; de Lorenzo, V. *J. Biol. Chem.* **2015**, *290*, 25920-25932.
(20) Simon, M. J.; Osslund, T. D.; Saunders, R.; Ensley, B. D.; Suggs, S.; Harcourt, A.; Suen, W. C.; Cruden, D. L.; Gibson, D. T.; Zylstra, G. J. *Gene* **1993**, *127*, 31-37.
(21) Franco, M. I.; Turin, L.; Mershin, A.; Skoulakis, E. M. C. *Proc. Natl. Acad. Sci. U. S. A.* **2011**, *108*, 3797-3802.
(22) Romano, A. H.; Conway, T. *Res. Microbiol.* **1996**, *147*, 448-455.
(23) Sudarsan, S.; Dethlefsen, S.; Blank, L. M.; Siemann-Herzberg, M.; Schmid, A. *Appl. Environ. Microbiol.* **2014**, *80*, 5292-5303.
(24) Kahlon, R. S. *Pseudomonas: Molecular and Applied Biology*; Springer, 2006, p 110-118.
(25) Harwood, C. S.; Parales, R. E. *Annu. Rev. Microbiol.* **1996**, *50*, 553-590.
(26) Murinova, S.; Dercova, K. *Int. J. Microbiol.* **2014**, *2014*, 873081.
(27) Mrozik, A.; Labuzek, S.; Piotrowska-Seget, Z. *Microbiol. Res.* **2005**, *160*, 149-157.
(28) Mrozik, A.; Piotrowska-Seget, Z.; Labuzek, S. *Microbiol. Res.* **2004**, *159*, 87-95.
(29) Keweloh, H.; Diefenbach, R.; Rehm, H. J. *Arch. Microbiol.* **1991**, *157*, 49-53.
(30) Heipieper, H. J.; Weber, F. J.; Sikkema, J.; Keweloh, H.; de Bont, J. A. M. *Trends Biotechnol.* **1994**, *12*, 409-415.
(31) Selvarasu, S.; Ow, D. S.; Lee, S. Y.; Lee, M. M.; Oh, S. K.; Karimi, I. A.; Lee, D. Y. *Biotechnol. Bioeng.* **2009**, *102*, 923-934.
(32) Entner, N.; Doudoroff, M. *J. Biol. Chem.* **1952**, *196*, 853-862.
(33) Vicente, M.; Canovas, J. L. *J. Bacteriol.* **1973**, *116*, 908-914.
(34) del Castillo, T.; Ramos, J. L.; Rodriguez-Herva, J. J.; Fuhrer, T.; Sauer, U.; Duque, E. *J Bacteriol.* **2007**, *189*, 5142-5152.
(35) Song, Y. Z.; Kaster, A. K.; Vollmers, J.; Song, Y. Q.; Davison, P. A.; Frentrup, M.; Preston, G. M.; Thompson, I. P.; Murrell, J. C.; Yin, H. B.; Hunter, C. N.; Huang, W. E. *Microb. Biotechnol.* **2017**, *10*, 125-137.
(36) McClure, N. C.; Weightman, A. J.; Fry, J. C. *Appl. Environ. Microbiol.* **1989**, *55*, 2627-2634.

Table 1. Strains and plasmids used in this study

Strain/plasmid	Description	Reference
Escherichia coli DH5α	*F⁻ φ80lacZΔM15 Δ(lacZYA-argF)U169 recA1 endA1 hsdR17(r_k- , m_k^+) phoA supE44 thi-1 gyrA96 relA1 λ⁻*	Invitrogen UK
Pseudomonas putida UWC1	Mutant of *Pseudomonas putida* KT2440; Rip^R, Rifampicin resistant, able to glucose as sole carbon source	[19,36]
Pseudomonas putida G7	Naphthalene degradation bacterium with plasmid NAH7, cannot use glucose as sole carbon source	[20]
Pseudomonas fluorescens WH2	Naphthalene degradation bacterium with plasmid pWH2-Nah	[9]
Pseudomonas putida UWC1 (pWH2-Nah^+)	Transconjugant of *Pseudomonas putida* UWC1 bearing the pWH2-Nah plasmid from *Pseudomonas fluorescens* WH2	This study
pWH2-Nah	Naphthalene degradation plasmid of *Pseudomonas fluorescens* WH2	[9]

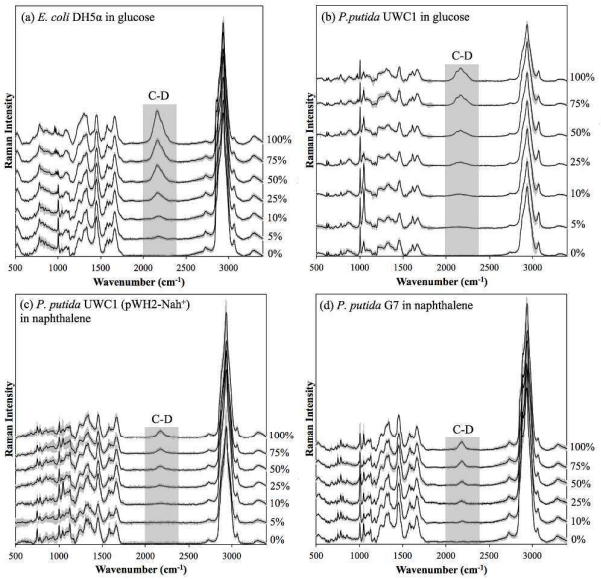

Figure 1. Single-cell Raman spectra (SCRS) of (a) *E. coli* DH5α and (b) *P. putida* UWC1 grown in glucose with different ratios of deuterated glucose-d_{12}. (c) *P. putida* UWC1 (pWH2-Nah^+) and (d) *P. putida* G7 grown in naphthalene with different ratios of deuterated naphthalene-d_8. The characteristic C-D Raman band centred at 2170 cm^{-1} is highlighted and it increases in intensity with increasing deuteration of the carbon source in all cases. Each spectrum is an average of 30 single-cell Raman spectra and the shaded area represents the standard deviation of the spread in single-cell measurements.

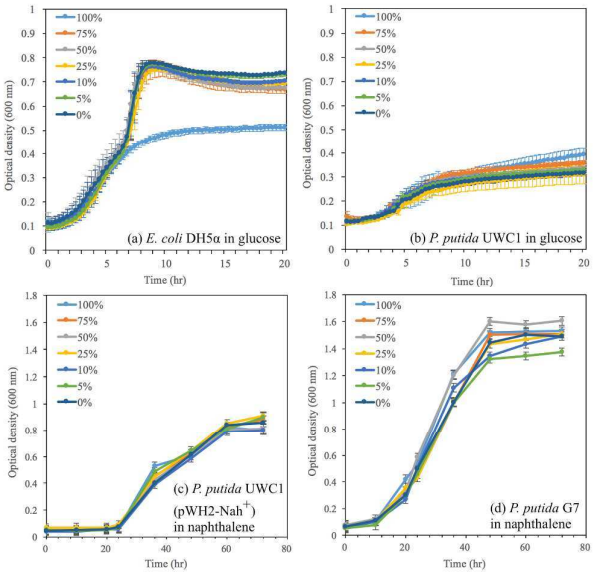

Figure 2. Growth curves were created by OD_{600} measurements of cultures of (a) *E. coli* DH5α and (b) *P. putida* UWC1 grown in M9 with different ratios of deuterated glucose-d_{12}, (c) *P. putida* UWC1 (pWH2-Nah^+) and (d) *P. putida* G7 grown in M9 with different ratios of deuterated naphthalene-d_8. *E. coli* DH5α using 100% glucose-d_{12} displays a similar log growth phase but an inhibited stationary phase compared to other deuterated conditions. All OD_{600} of *P. putida* UWC1, *P. putida* UWC1 (pWH2-Nah^+) and *P. putida* G7 before and after incubation show no significant difference ($p > 0.01$) among conditions with 0% to 100% naphthalene-d_8.

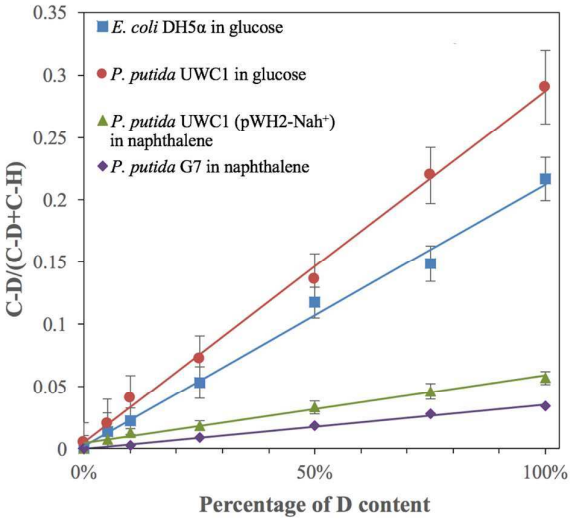

Figure 3. Comparison of the percentage of D content in carbon source with the band intensity ratio of C-D / (C-D + C-H) in SCRS of *E. coli* DH5α and *P. putida* UWC1 grown in glucose, and of *P. putida* UWC1 (pWH2-Nah$^+$) and *P. putida* G7 grown in naphthalene, with different percentages of glucose-d_{12} or naphthalene-d_8. All conditions show a linearity between carbon source D percentage and cellular D incorporation. However, bacterial cells grown with naphthalene have a significant lower D incorporation compared to cells grown with glucose ($p < 0.001$).

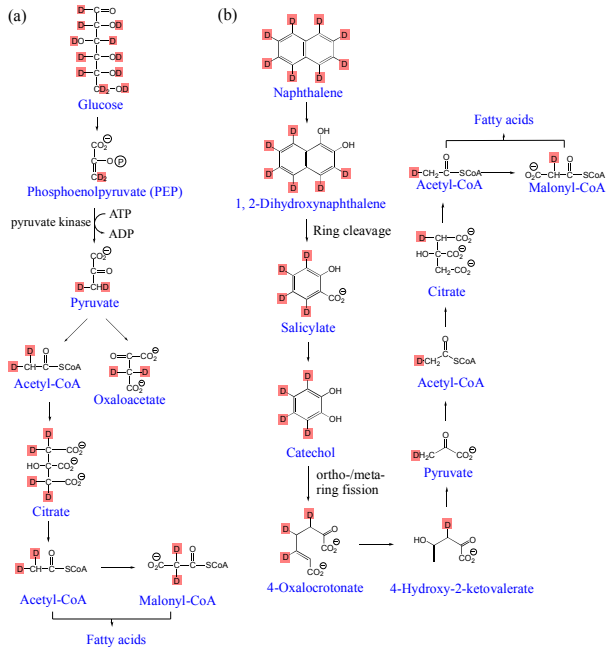

Figure 4. Fatty acids metabolic pathways starting from (a) deuterated glucose and (b) deuterated naphthalene. In both pathways, deuterated carbon source degradation leads to production of deuterated fatty acids and is therefore responsible for the shift from C-H (2800 - 3030 cm^{-1}) to C-D (2070 - 2300 cm^{-1}). Pathway (b) shows dilution of D in naphthalene catabolism during degradation of the aromatic ring.

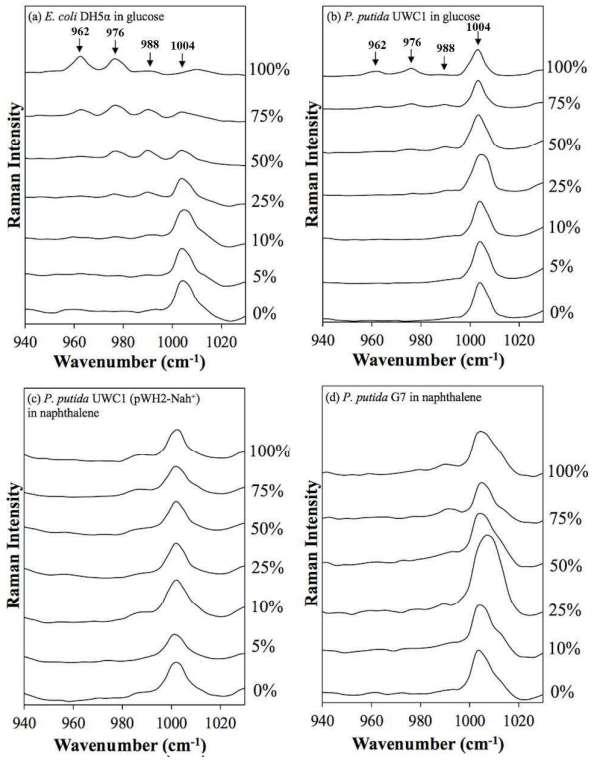

Figure 5. Enlarged view of phenylalanine shifts from 1004 cm^{-1} to 988, 976 and 962 cm^{-1} in the Raman spectra with respect to different ratios of deuterated growth glucose-d_{12} or naphthalene-d_8. Each spectrum is an average of 30 single-cell Raman spectra.

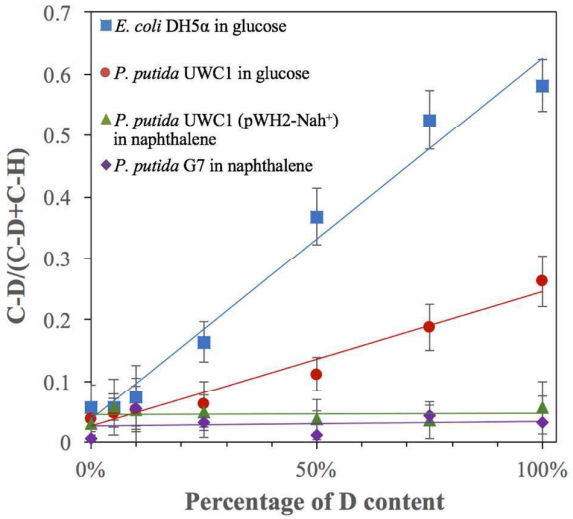

Figure 6. Comparison of D content in phenylalanine band of SCRS of *E. coli* DH5α and *P. putida* UWC1 grown in glucose, and *P. putida* UWC1 (pWH2-Nah$^+$) and *P. putida* G7 grown in naphthalene with respect to different percentages of deuterated glucose-d_{12} or naphthalene-d_8. Both glucose conditions show a linearity between carbon source D percentage and cellular D incorporation. However, no D incorporation is observed in bacterial cells grown with naphthalene.

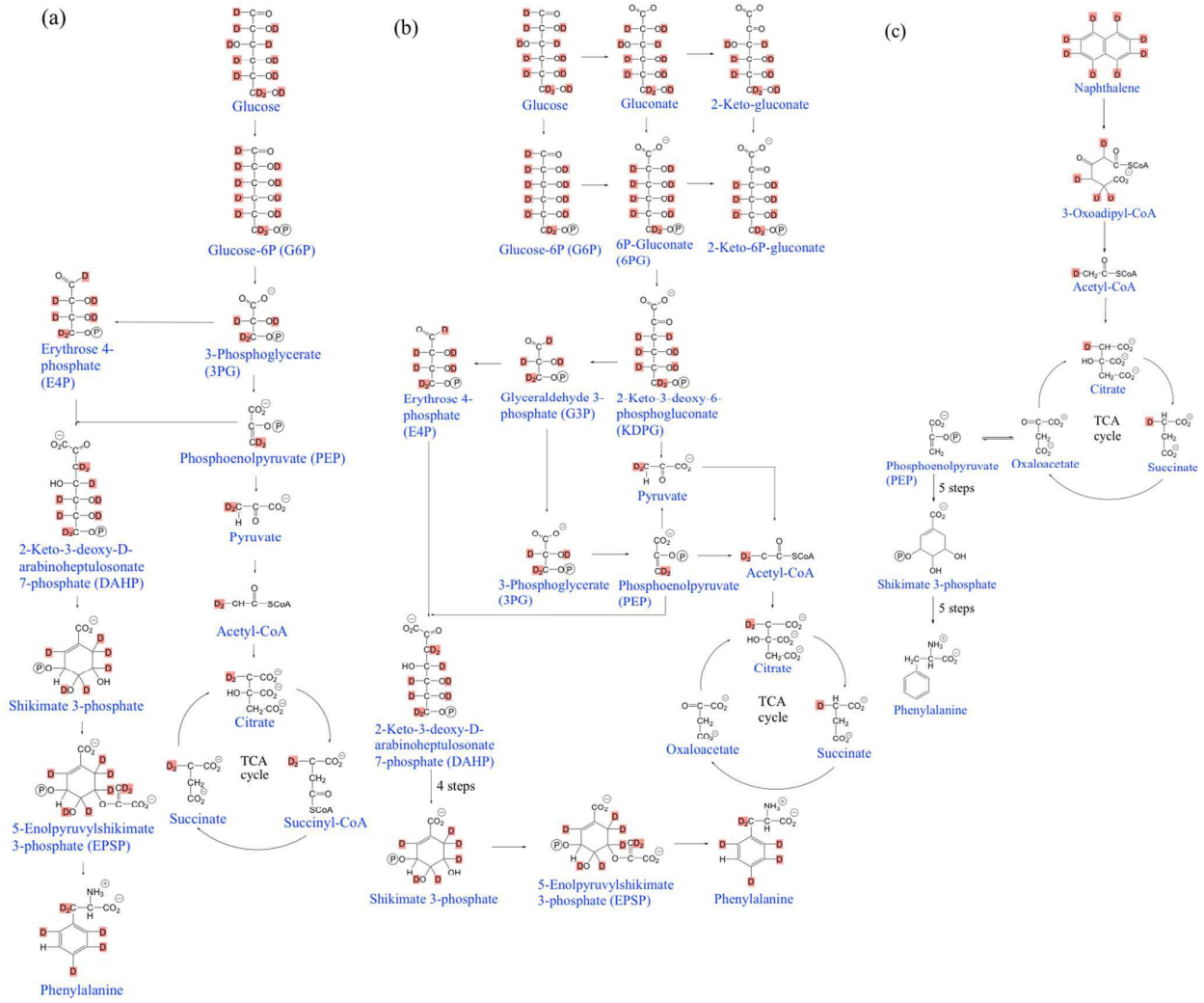

Figure 7. Phenylalanine metabolic pathway of (a) *E. coli* grown in glucose, (b) *P. putida* UWC1 grown in glucose, and (c) *P. putida* UWC1 (pWH2-Nah^{+}) grown in naphthalene. Pathway (b) shows the three simultaneous sub-pathways in *Pseudomonas* using deuterated glucose, which might contribute to the observed less D incorporation compared to *E. coli*. Pathway (c) suggests little D incorporation from deuterated naphthalene degradation due to dilution of D during the two-phase ring breaking processes and in the TCA cycle.

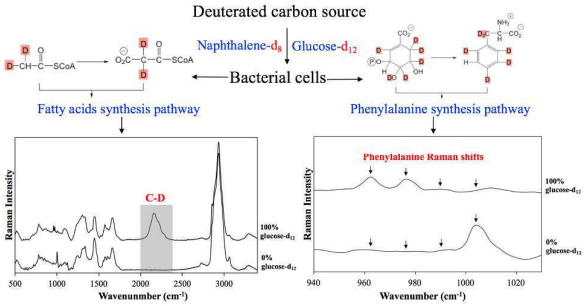
Deuterated carbon source
Naphthalene-d8
Glucose-d12
Bacterial cells
Fatty acids synthesis pathway
Phenylalanine synthesis pathway
C-D
Raman Intensity
Wavenumber (cm-1)
Phenylalanine Raman shifts
100% glucose-d12
0% glucose-d12

For TOC only.